Hindawi
Shock and Vibration
Volume 2019, Article ID 2984191, 10 pages
https://doi.org/10.1155/2019/2984191

Research Article

Numerical and Experimental Studies on Inclined Incidence Parametric Sound Propagation

Haisen Li,[1,2,3] Jingxin Ma,[1,3] Jianjun Zhu,[1,2,3] and Baowei Chen[1,2,3]

[1]*Acoustic Science and Technology Laboratory, Harbin Engineering University, Harbin 150001, China*
[2]*Key Laboratory of Marine Information Acquisition and Security (Harbin Engineering University), Ministry of Industry and Information Technology, Harbin 150001, China*
[3]*College of Underwater Acoustic Engineering, Harbin Engineering University, Harbin 150001, China*

Correspondence should be addressed to Jianjun Zhu; zhujianjun_heu@hrbeu.edu.cn

Received 26 July 2019; Revised 7 October 2019; Accepted 1 November 2019; Published 20 November 2019

Academic Editor: Rui Moreira

The Khokhlov–Zabolotskaya–Kuznetsov (KZK) equation has been widely used in the simulation and calculation of nonlinear sound fields. However, the accuracy of KZK equation reduced due to the deflection of the direction of the sound beam when the sound beam is inclined incidence. In this paper, an equivalent sound source model is proposed to make the calculation direction of KZK calculation model consistent with the sound propagation direction after acoustic refraction, so as to improve the accuracy of sound field calculation under the inclined incident conditions. The theoretical research and pool experiment verify the feasibility and effectiveness of the proposed method.

1. Introduction

Due to the nonlinear effect of the medium, when the parametric acoustic array transmitted two similar frequency primary sound waves, the difference, sum, and harmonic frequency waves will be generated in the radiated sound field [1–3]. The parametric array technology can generate broadband, high directivity, and side-lobe suppressed low-frequency sound beams by using a small aperture array [4–6]. This parametric sound feature makes the parametric sonar more suitable for high-directivity sound beam noninvasive measurement and high-resolution sub-bottom profiling [7–9]. When the parametric sound is obliquely irradiated into different media, the acoustic propagation path changes due to the medium parameters, which has a certain influence on the application of the parametric sound. Such as the direction of sound propagation will be deflected when the high-intensity focused ultrasound used in the noninvasive treatment of solid tumors and inversion error of shallow depth parameter due to inclined seabed.

As the most accurate mathematical equation describing the nonlinear sound field, the KZK equation is the most important mathematical tool for the study of acoustic propagation in various media layers [10]. For the problem of parametric sound transmission in near-field, finite-difference frequency-domain method (FDFD) and finite-difference time-domain method (FDTD) were proposed to calculate parametric sound propagation [11–14]. Several numerical and experimental results for the parametric sound field propagation characteristics based on circular parametric array were found [15–18]. However, most of the parametric array equipment used in underwater acoustics detection area is rectangular due to production process conditions. In [19], the KZK equation in the Cartesian coordinate system under the rectangular aperture parameter sound source condition is proposed, and both natural directivity and phase control parametric sound source in free field were numerically simulated. Vander Meulen and Haumesser constructed the model of finite amplitude sound beam propagation for the vertical incident baffle, and the nonlinearity coefficient of the aluminum plate medium has been measured and evaluated by the in-depth analysis of the second harmonic in the sound field [20]. Fujisawa and Asada numerically and experimentally examined the parametric sound field when the sound beams through different fluid layers vertically and proposed a nonlinear parametric sound

enhancement method by placing a highly nonlinear coefficient of fluid layer in front of the parametric array [21]. However, the numerical model of the parametric sound beam through the medium with different angles research is rarely carried out.

In this paper, under a rectangular aperture parameter source, based on the KZK equation, a theoretical model of the inclined incidence parametric sound field is proposed and constructed. The parametric sound field after inclined incidence of aluminum plates and different media is studied, respectively. Finally, the results of the aluminum plate were verified by the pool test.

2. Theory Equation and Geometry Model

2.1. Governing Equation. As an extended form of the Burgers model, the KZK equation is the most accurate equation model for calculating the paraxial region of a nonlinear sound field. The KZK equation defined in the Cartesian rectangular coordinates can be described as follows [19]:

$$\frac{\partial^2 p}{\partial z\,\partial t'} = \frac{c_0}{2}\left(\frac{\partial^2}{\partial x^2} + \frac{\partial^2}{\partial y^2}\right)p + \frac{\delta}{2c_0^3}\frac{\partial^3 p}{\partial t'^3} + \frac{\beta}{2\rho_0 c_0^3}\frac{\partial^2 p^2}{\partial t'^2}, \quad (1)$$

where p is the sound pressure, c_0 is the sound velocity, ρ_0 is the medium density, δ is the diffusivity of sound, β is the nonlinearity coefficient, and $t' = t - z/c_0$ is the time delay at z with t being the time.

By using the Lee and Hamilton method [12], equation (1) can be transformed into nondimensional form by coordinate transformation to improve the computational efficiency. The transformation parameters are as follows:

$$\begin{aligned} \sigma &= \frac{z}{R_0}, \\ u_x &= \frac{x}{[a(1+\sigma)]}, \\ u_y &= \frac{y}{[b(1+\sigma)]}, \\ P &= \frac{p(1+\sigma)}{p_0}, \\ \tau &= \frac{\omega_0 t' - k_0(x^2+y^2)}{[2R_0(1+\sigma)]}. \end{aligned} \quad (2)$$

The dimensionless form of the KZK equation can be written as

$$\frac{\partial P}{\partial \sigma} = \frac{R}{\pi(1+\sigma)^2}\int_{-\infty}^{\tau}\left(\frac{\partial^2 P}{\partial u_x^2} + \frac{\partial^2 P}{\partial u_y^2}\right)d\tau' + \alpha_0 R_0 \frac{\partial^2 P}{\partial \tau^2} + \frac{NP}{1+\sigma}\frac{\partial P}{\partial \tau}, \quad (3)$$

where $\alpha_0 = \delta\omega_0^2/(2c_0^3)$ is the absorption coefficient, $R_0 = 4ab/\lambda$ is the Rayleigh distance, $N = (\beta p_0 \omega_0 R_0)/(\rho_0 c_0^3)$ is the nonlinear coefficient in dimensionless form, p_0 is input sound pressure, ω_0 is the angular frequency, k_0 is the wave number, $R = b/a$ is the aspect ratio, and the parametric source dimension is $2a \times 2b$ $(a \geq b)$.

2.2. Equivalent Source Incident Numerical Model. When the parametric sound field is incident obliquely into another medium, the beam direction will deviate due to the acoustic refraction effect. At this time, an equivalent parametric sound source coordinate system is established such that the acoustic refraction parametric sound field is considered to be generated by the equivalent parametric sound source. As shown in Figure 1(b), the new transformed coordinate system (u_x^1, u_y^1, σ^1) is introduced in region Ω_1 to be consistent with the direction of sound line propagation. The coordinates of the center position of the inclined interface are $(0, \sigma_0^0 = z_0/R_0)$ and $(0, \sigma_0^1)$, respectively, in the two coordinate systems.

Under the transformed coordinate system constructed under the condition of equation (2), the coordinate parameter scale is related to the Rayleigh distance. Therefore, not only the acoustic parameters are different in new media but also the dimensionless coordinate system's coordinate scale. The relationship between the two coordinate systems in the axial direction is as follows:

$$\begin{bmatrix} \Delta\sigma^1 \\ \sigma^1 \end{bmatrix} = \begin{bmatrix} \dfrac{\Delta\sigma^0 (R_0/R_1)}{\cos\alpha} \\ \dfrac{(R_0/R_1)(\sigma^0 - \sigma_0^0)}{\cos\alpha} + \sigma_0^1 \end{bmatrix}, \quad (4)$$

where R_1 is the Rayleigh distance in the new media and $\alpha = \theta_0 - \arcsin(c_1/c_0 \cdot \sin(\theta_0))$ is the angle of acoustic refraction deflection.

As shown in Figure 1(b), any point (x, y, z) on the inclined plane can be transformed into two nondiffusion coordinate systems with equation (2), respectively, which are

$$\begin{aligned} u_x^0 &= -\frac{R_0}{\tan\theta}\cdot\frac{\sigma^0 - \sigma_0^0}{a(1+\sigma^0)}, \\ u_x^1 &= -\frac{R_1}{\tan(\theta-\alpha)}\cdot\frac{\sigma^1 - \sigma_0^1}{a(1+\sigma^1)}. \end{aligned} \quad (5)$$

Analyzing the relationship of u_x^0 and u_x^1 by equation (4), we can get

$$\begin{aligned} \frac{u_x^1}{u_x^0} &= \frac{R_1\tan\theta}{R_0\tan(\theta-\alpha)}\cdot\frac{\sigma^1 - \sigma_0^1}{\sigma^0 - \sigma_0^0}\cdot\frac{1+\sigma^0}{1+\sigma^1} \\ &= \frac{R_1\tan\theta}{R_0\tan(\theta-\alpha)}\cdot\frac{1+\sigma^0}{(R_1/R_0)(1+\sigma_0^1)\cos\alpha - \sigma_0^0 + \sigma^0}. \end{aligned} \quad (6)$$

To simplify the complexity of the model coordinate system transformation, it is assumed that the coordinates of the points on inclined plane are linear in the two coordinate systems, in which the value of σ_0^1 can be set as

$$\sigma_0^1 = \frac{R_0}{R_1\cos\alpha}\left(1+\sigma_0^0\right) - 1. \quad (7)$$

The relationship between the coordinate-scale transformation in the new coordinate system and the original coordinate system on inclined plane is

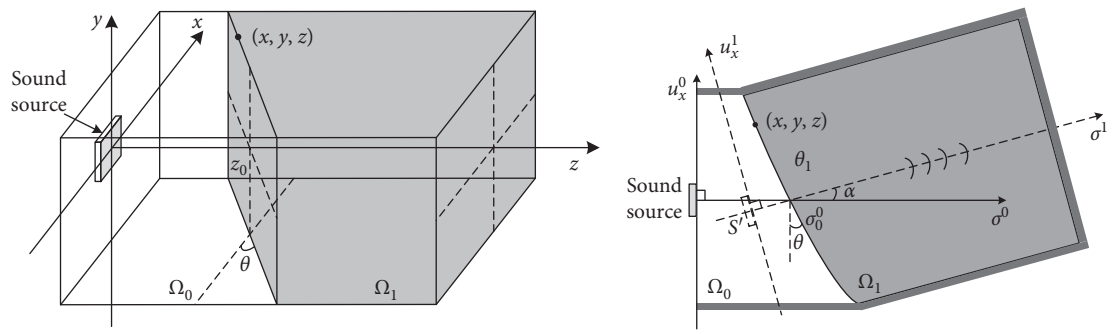

Figure 1: Schematic diagram of nonlinear acoustic propagation under inclined incidence conditions. (a) Cartesian rectangular coordinates. (b) Dimensionless transformed coordinate system.

$$\begin{bmatrix} \Delta u_x^1 \\ \Delta u_y^1 \\ \Delta \sigma^1 \end{bmatrix} = \begin{bmatrix} \dfrac{R_1 \tan\theta}{[R_0 \tan(\theta-\alpha)] \cdot \Delta u_x^0} \\ \dfrac{R_1 \tan\theta}{[R_0 \tan(\theta-\alpha)] \cdot \Delta u_y^0} \\ \dfrac{R_0}{(R_1 \cos\alpha) \cdot \Delta \sigma^0} \end{bmatrix}. \tag{8}$$

The transformation relationship between the two coordinate systems on inclined plane is

$$\begin{bmatrix} u_x^1 \\ u_y^1 \\ \sigma^1 \end{bmatrix} = \begin{bmatrix} \dfrac{R_1 \tan\theta}{[R_0 \tan(\theta-\alpha)] \cdot u_x^0} \\ \dfrac{R_1 \tan\theta}{[R_0 \tan(\theta-\alpha)] \cdot u_y^0} \\ \dfrac{(R_0/R_1)(\sigma^0 - \sigma_0^0)}{\cos\alpha + \sigma_0^1} \end{bmatrix}. \tag{9}$$

Therefore, the coordinate system (u_x^1, u_y^1, σ^1) in Figure 1(b) can be transformed back to the Cartesian coordinate system (x, y, z) in Figure 1(a) with

$$\begin{bmatrix} x \\ y \\ z \end{bmatrix} = \begin{bmatrix} a\cos\alpha & 0 & -R_1 \sin\alpha \\ 0 & b & 0 \\ \sin\alpha & 0 & R_1 \cos\alpha \end{bmatrix} \begin{bmatrix} (1+\sigma^1)u_x^1 \\ (1+\sigma^1)u_y^1 \\ \sigma^1 - \sigma_0^1 \end{bmatrix} + \begin{bmatrix} 0 \\ 0 \\ z_0 \end{bmatrix}. \tag{10}$$

2.3. Boundary Condition. Figure 1 shows the sound field computational domain, which is set as $10 \times 10 \times 100$ in the u_x, u_y, and σ directions, respectively. Around the computational domain, an absorbing boundary condition is imposed to minimize the acoustic reflections from the edges. The entire computational sound field is divided into two water areas (Ω_0 and Ω_1) by the inclined plane. The inclined plane section is perpendicular to the x-o-z plane and is at an angle of θ to the plane x-o-y, and the center of the section is at a horizontal distance z_0 from the parametric source.

For the sound pressure calculation, in natural parametric sound field, the sound source on $z = 0$ is used as an initial condition prescribed by two different primary frequencies as follows:

$$P_0 = p_0(\cos 2\pi f_1 t + \cos 2\pi f_2 t), \tag{11}$$

where $f_1 = (f_0 - f_d/2)$ and $f_2 = (f_0 + f_d/2)$ are the two primary frequencies of parametric source, f_0 and f_d are the center and difference frequencies of the primary waves, respectively, and t is the time. After the parameter transformation, two different primary frequencies in simulation calculation are as follows:

$$P_0(u_x, u_y) = p_0 \left\{ \cos\left[2\pi f_1 \tau + \frac{\pi(u_x^2 + u_y^2)}{4}\right] + \cos\left[2\pi f_2 \tau + \frac{\pi(u_x^2 + u_y^2)}{4}\right] \right\} \cdot H(u_x, u_y), \tag{12}$$

where

$$H(u_x, u_y) = \begin{cases} 1, & |u_x| \le 1, |u_y| \le R, \\ 0, & \text{other.} \end{cases} \tag{13}$$

Since the KZK equation describes only the unidirectional propagation of the nonlinear parametric sound field, the reflected sound beam is not considered in the actual calculation. At the water-ethanol boundary, there is a thin rubber film with the same acoustic impedance as water to prevent any mixing of ethanol and water. And, the sound pressure transmission coefficient of the water-ethanol boundary and the water-aluminum boundary, respectively, is as follows:

$$T_{\mathrm{WE}} = \frac{(2\rho_{\mathrm{E}} c_{\mathrm{E}})/\cos\theta}{(\rho_{\mathrm{E}} c_{\mathrm{E}})/\cos\theta + (\rho_{\mathrm{W}} c_{\mathrm{W}})/\cos(\theta-\alpha)},$$

$$T_{\mathrm{WA}} = \frac{2Z_{\mathrm{W}} Z_{\mathrm{A}}}{2Z_{\mathrm{W}} Z_{\mathrm{A}} \cos(k_{\mathrm{A}} l \cos\theta_{\mathrm{A}}) + j(Z_{\mathrm{W}}^2 + Z_{\mathrm{A}}^2)\sin(k_{\mathrm{A}} l \cos\theta_{\mathrm{A}})}, \tag{14}$$

where $Z_{\mathrm{W}} = (\rho_{\mathrm{W}} c_{\mathrm{W}})/\cos\theta$, $Z_{\mathrm{E}} = (\rho_{\mathrm{E}} c_{\mathrm{E}})/\cos(\theta-\alpha)$, θ_{A} is the refraction angle in the aluminum plate, k_{A} is the wave

number in aluminum, and l is the thickness of the thin aluminum plate. The subscripts E, A, and W represent ethanol, aluminum, and water, respectively. The parameters used in this study are given in Table 1.

2.4. Numerical Algorithm. In the nonlinear sound field numerical analysis, the KZK equation was solved with the finite-difference time-domain method (FDTD) for the acoustic field from a rectangular aperture parameter array source. The staggered grid system at inclined plane boundary is described in Figure 2. The four terms on the right side of equation (1) represent diffraction in u_x, u_y axial directions, attenuation, and nonlinearity, respectively. Based on an orthogonal spatial grid, each term of the equation can be calculated as independent equation. The discretized forms of these equations are expressed as

Table 1: Density and sound speed values.

Material	Water	Ethanol	Aluminum
Density ρ (kg/m^3)	1000	785	2700
Speed c (m/s)	1473	1168	6300
Z_{mat} (Rayls)	1.47×10^6	9.17×10^5	1.7×10^7
Nonlinear coefficient β	3.5	6.9	—
Absorption coefficient ($10^{-13} f^2$ dB/m)	2.17	4.78	—

$$\frac{P_{m,n}^{j,k+1} - P_{m,n}^{j,k}}{\Delta\sigma_k} = \frac{R}{\pi(1+\sigma)^2} \int_{-\infty}^{\tau} \left(\frac{P_{m+1,n}^{j,k+1} - 2P_{m,n}^{j,k+1} + P_{m-1,n}^{j,k+1}}{2(\Delta u_x)^2} \right) d\tau', \tag{15}$$

$$\frac{P_{m,n}^{j,k+1} - P_{m,n}^{j,k}}{\Delta\sigma_k} = \frac{R}{\pi(1+\sigma)^2} \int_{-\infty}^{\tau} \left(\frac{P_{m,n+1}^{j,k+1} - 2P_{m,n}^{j,k+1} + P_{m,n-1}^{j,k+1}}{2(\Delta u_y)^2} \right) d\tau', \tag{16}$$

$$\frac{P_{m,n}^{j,k+1} - P_{m,n}^{j,k}}{\Delta\sigma_k} = \alpha_0 R_0 \frac{P_{m,n}^{j+1,k+1} - 2P_{m,n}^{j,k+1} + P_{m,n-1}^{j-1,k+1}}{\Delta\tau^2}, \tag{17}$$

$$P_{m,n}^{j,k+1} = \begin{cases} \dfrac{P_{m,n}^{j,k}}{1 - N\left[\left(P_{m,n}^{j+1,k} - P_{m,n}^{j,k}\right)/\Delta\tau\right]\ln\left[1 + (\Delta\sigma_k)/(1+\sigma_k)\right]}, & P_{m,n}^{j,k} \geq 0, \\ \dfrac{P_{m,n}^{j,k}}{1 - N\left[\left(P_{m,n}^{j,k} - P_{m,n}^{j-1,k}\right)/\Delta\tau\right]\ln\left[1 + (\Delta\sigma_k)/(1+\sigma_k)\right]}, & P_{m,n}^{j,k} < 0, \end{cases} \tag{18}$$

where m, n, and k are the spatial coordinate indexes in the u_x, u_y, and σ axial directions, respectively, and j is the time step. For example, $P_{m,n}^{j,k} = P(m \cdot \Delta u_x, n \cdot \Delta u_y, \sigma_k, j \cdot \Delta\tau)$.

Consider the effect of the slope boundary on the calculation of the discretization equation, as shown in Figure 2. The calculation parameters are different on both sides of the slope boundary in equations (16)–(18), but the calculation conditions are consistent with the free field. However, in equation (15), the inclined boundary divides the u_x-direction scattering calculation into two parts, as shown in Figure 2(b), and the approximate inclined boundary is

$$\frac{P_{m,n}^{j,k} - P_{m,n}^{j,k-1}}{\Delta\sigma_k} = \frac{R}{\pi(1+\sigma)^2} \int_{-\infty}^{\tau} \cdot \left(\frac{\left(P_{m+1,n}^{j,k}/T\right) - 2P_{m,n}^{j,k} + P_{m-1,n}^{j,k}}{2(\Delta u_x)^2} \right) d\tau'. \tag{19}$$

When the u_x-direction diffraction calculation is completed, the initial condition of sound pressure $P_m^{j,k}$ at inclined incidence boundary, as shown in Figure 2(a), can be defined as follows:

$$P_m^{j,k} = P_m^{j,k} \cdot T. \tag{20}$$

3. Simulation Results and Discussion

The distance between the center of the inclined plane in Figure 1 and the parametric sound source is $z_0 = 3$ m. $p_0 = 1 \times 10^{-6}$ Pa and SL = 239 dB. The rectangular parametric array was used as a sound source (the aperture is 0.22 m × 0.22 m). The transducer was excited by two different primary frequencies at $f_1 = 95$ kHz and $f_2 = 110$ kHz with the transmittance time of the signal 0.267 ms. The parameters used in this study are given in Table 1.

3.1. Sound Pressure Distribution. In order to better understand the inclined incidence mechanism of the parametric sound field, the numerical simulation of the acoustic field propagation of the parametric sound field under normal incidence and 30° angle incidence is carried out. The numerical calculation results of the water-aluminum boundary model are shown in Figure 3, and the water-ethanol boundary model results are shown in Figure 4.

Compared to the aluminum plate boundary in Figure 3, higher nonlinear parameters make the difference

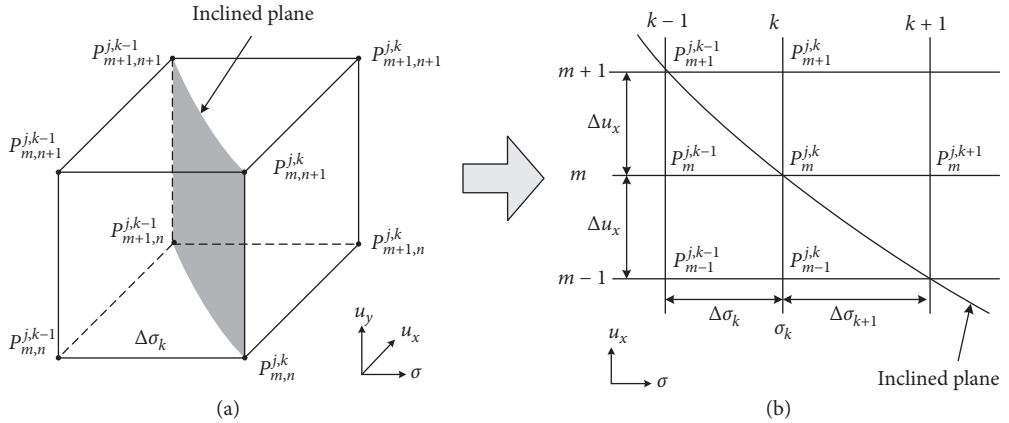

FIGURE 2: Finite-difference method staggered grid system. (a) Staggered grid system at inclined boundary. (b) Staggered grid system in x-directions represent diffraction.

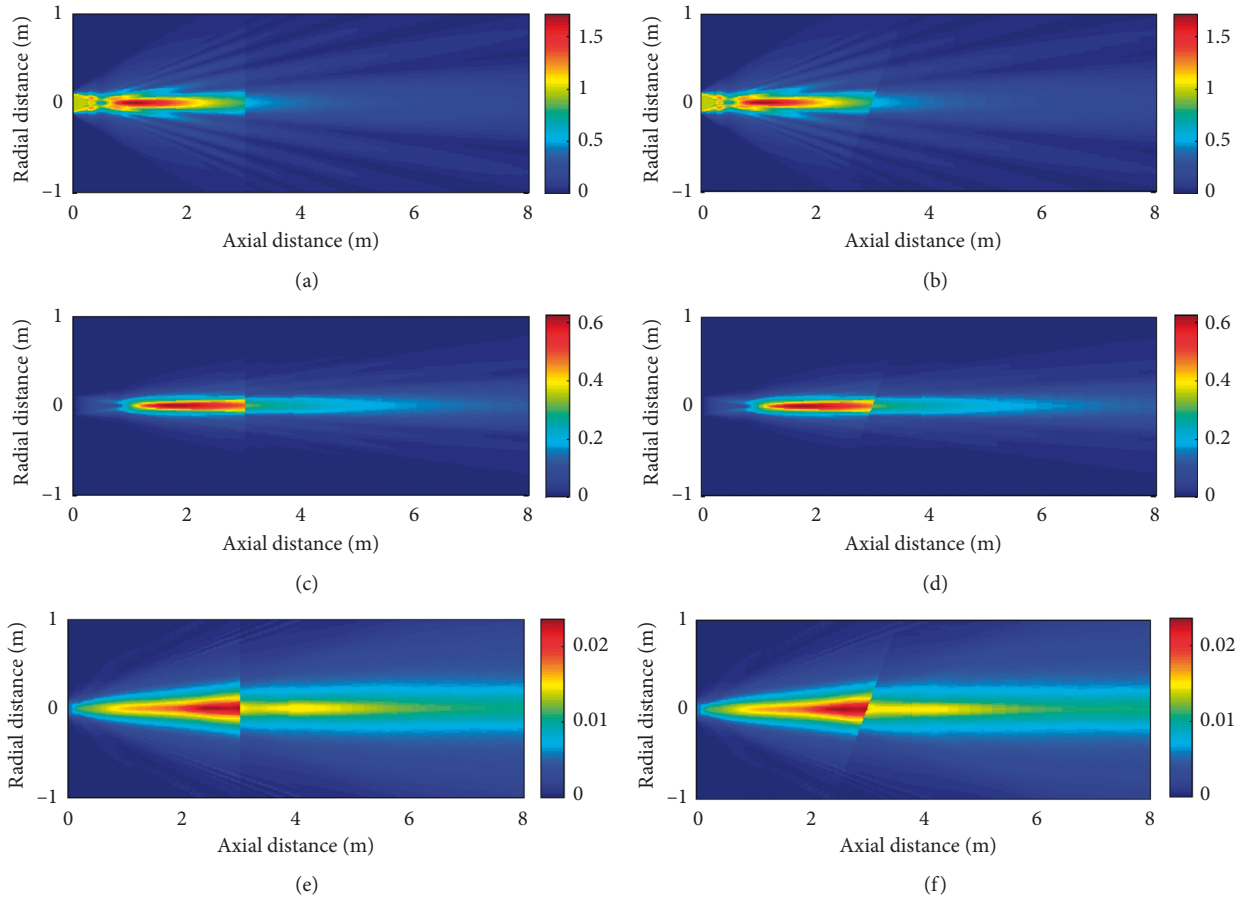

FIGURE 3: Simulated sound pressure distribution with the different angle incident water-aluminum boundary models. (a) $f = 95$ kHz, $\theta = 0°$; (b) $f = 95$ kHz, $\theta = 30°$; (c) $f = 205$ kHz, $\theta = 0°$; (d) $f = 205$ kHz, $\theta = 30°$; (e) $f = 15$ kHz, $\theta = 0°$; (f) $f = 15$ kHz, $\theta = 30°$.

frequency sound in the ethanol medium have a distinct sound enhancement process. In Figures 4(b), 4(d), and 4(f), the sound propagation direction in ethanol medium deflects 6.66° due to the refraction effect. The difference frequency and the sum frequency sound still maintain good symmetry in the direction of sound propagation.

3.2. Simulation Results of Sound Pressure Distribution. In the sound field calculation units at the inclined boundary sound field area, the whole sound field is divided into Ω_0 and Ω_1 areas by the inclined plane, where areas Ω_0 and Ω_1, respectively, are before and after the boundary region of the inclined plane. Figure 5 shows the 2D sound pressure distribution at σ_0 away from the sound source in which the sound pressure amplitude

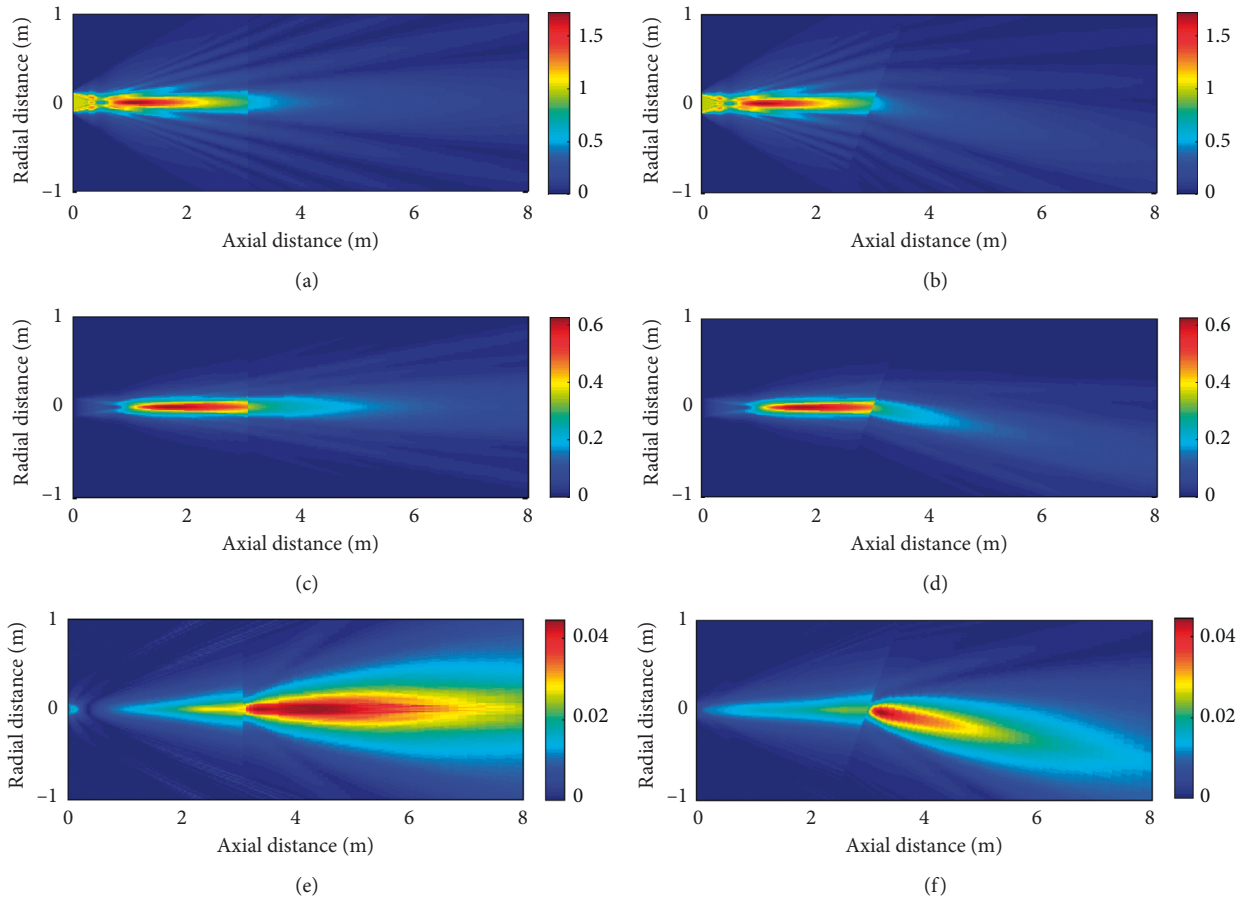

Figure 4: Simulated sound pressure distribution with the different angle incident water-ethanol boundary models. (a) $f = 95$ kHz, $\theta = 0°$; (b) $f = 95$ kHz, $\theta = 30°$; (c) $f = 205$ kHz, $\theta = 0°$; (d) $f = 205$ kHz, $\theta = 30°$; (e) $f = 15$ kHz, $\theta = 0°$; (f) $f = 15$ kHz, $\theta = 30°$.

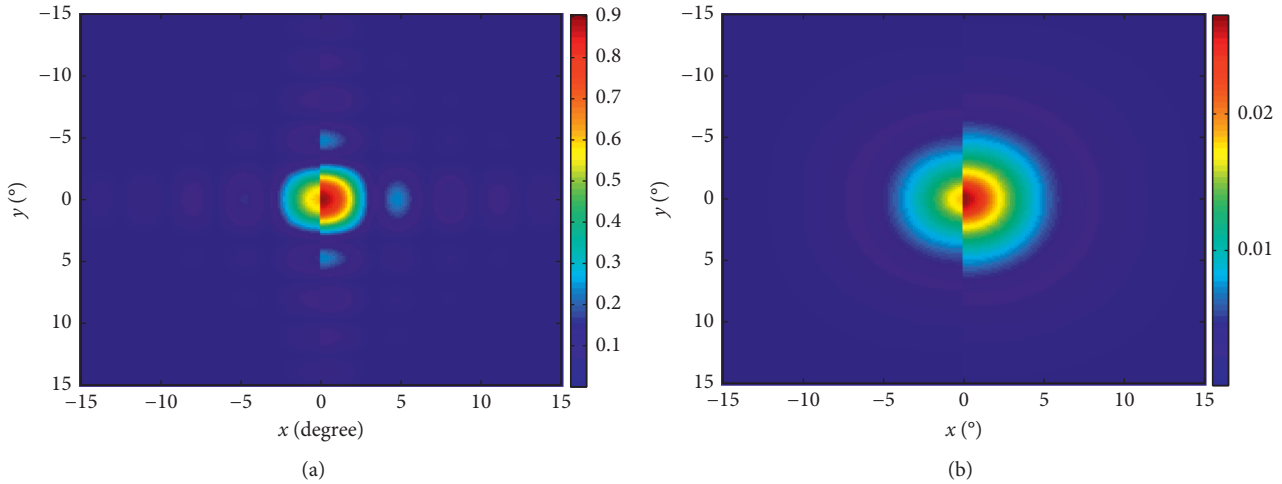

Figure 5: Continued.

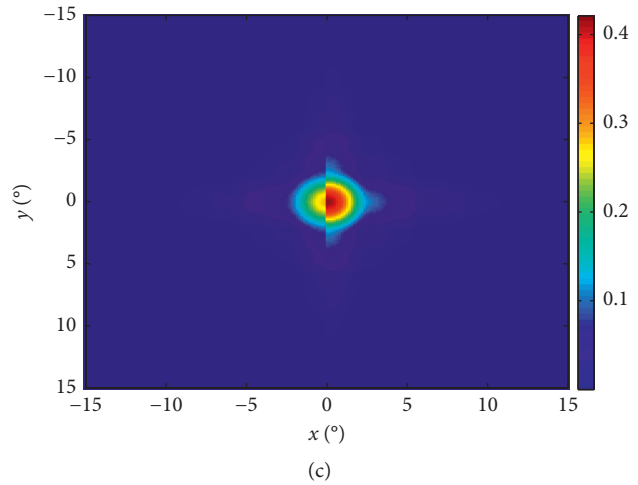

Figure 5: 2D sound pressure distribution at the center of water-ethanol boundary position ($z_0 = \sigma_0 R_0 = 3$ m). (a) Primary frequency; (b) difference frequency; (c) sum frequency.

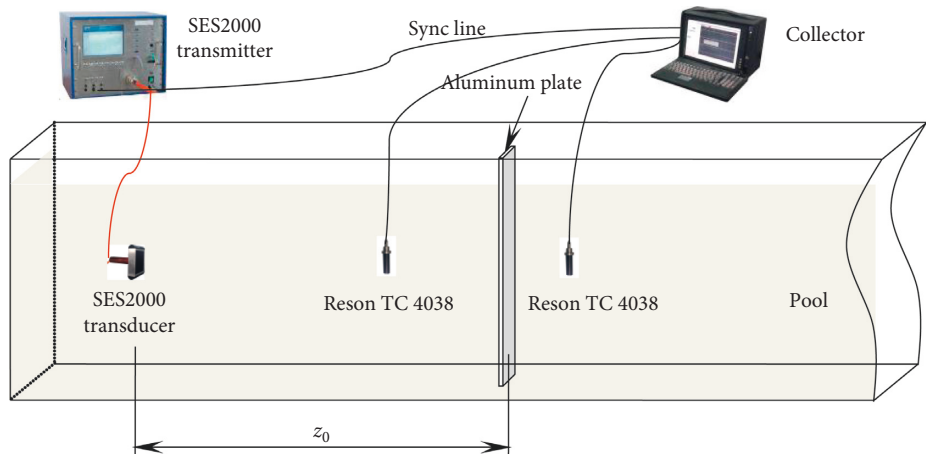

Figure 6: Experimental setup for the measurement of sound propagation through inclined plane.

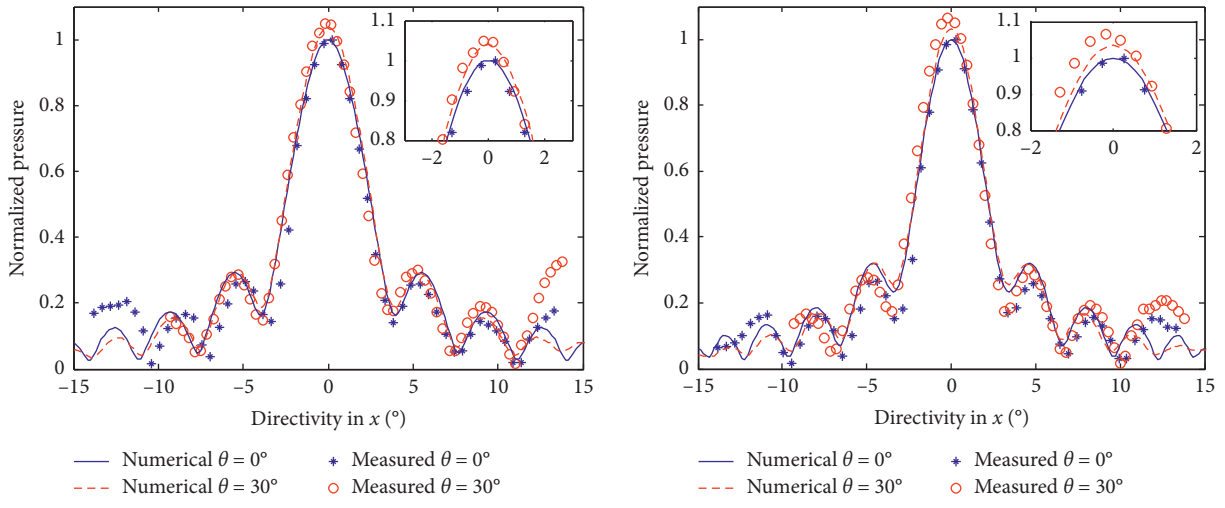

Figure 7: Continued.

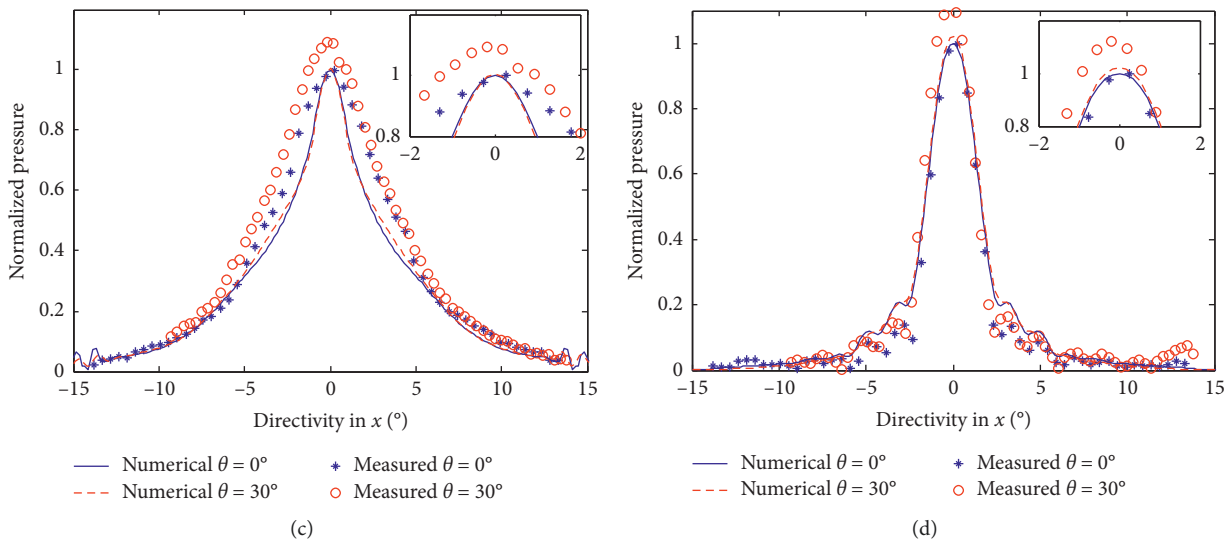

FIGURE 7: The directivity of sound pressure at 4 m away from the sound source with aluminum plate. (a) The primary sound pressure $f = 95$ kHz; (b) the primary sound pressure $f = 110$ kHz; (c) the difference frequency sound pressure $f = 15$ kHz; (d) the sum frequency sound pressure $f = 205$ kHz.

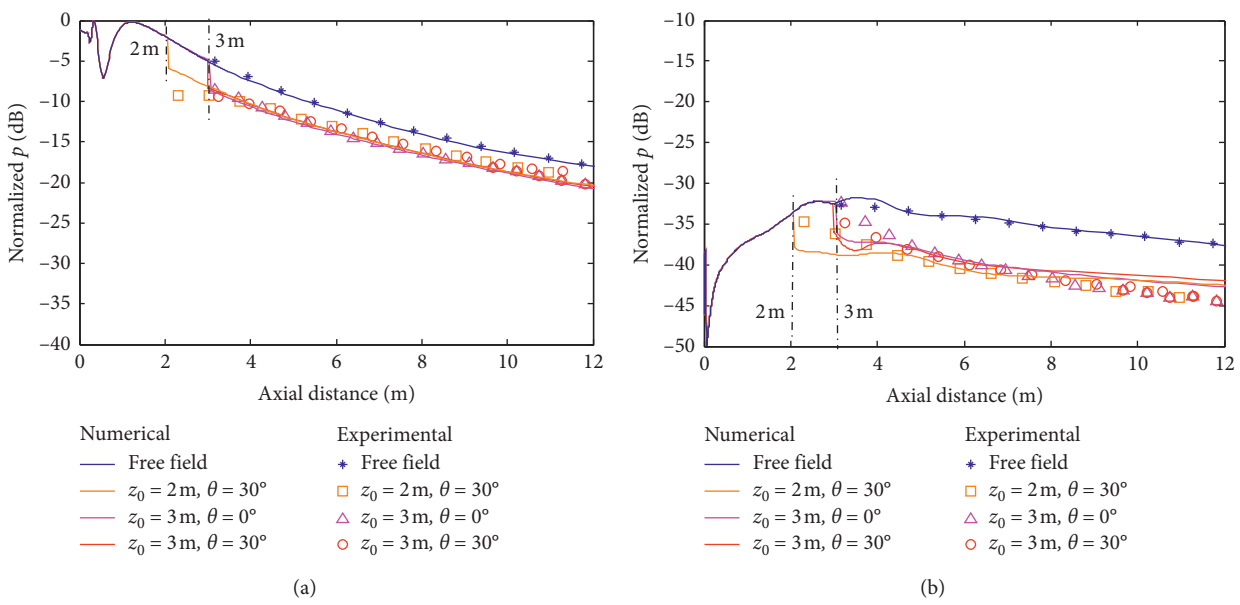

FIGURE 8: The axial sound pressure distribution of sound pressure. (a) The primary sound pressure $f = 95$ kHz. (b) The difference frequency sound pressure $f = 15$ kHz.

is normalized to the sound source's primary frequency value. All sound beams are symmetric in the y direction, and the sound pressure in Ω_1 is significantly smaller than the sound pressure in Ω_0 due to the inclined plane's sound pressure sound transmission coefficient. The acoustic beam of the primary frequency, as shown in Figure 5(a), forms distinct side lobes in the horizontal and vertical directions, while the difference and sum frequency sound beam has no side lobes.

4. Experimental Results and Discussion

4.1. Experimental Setup. To confirm the numerical results, the sound pressure distributions at primary, sum, and difference frequencies through inclined plane were measured using a TC4038 hydrophone, as shown in Figure 6. The water pool used in the experiments was 20 m long, 6 m wide, and 5 m deep (with the sound-absorbing tip around except the surface and bottom). The German SES2000 parametric array (0.22 m × 0.22 m) was used as a rectangular sound source, and the signal is collected by Tuopu's multichannel dynamic signal acquisition analyzer. In the experiment, the hydrophone was rigidly connected to the pool driving and the speed was set to 2 cm/s. A thin aluminum plate having a size of 2 m × 2 m and $l = 2.0$ mm thickness is used as the inclined transmission plane.

4.2. Inclined Plate Experimental Validations. The experimental study on the acoustic propagation characteristics of the parametric sound field under vertical and inclined incidence conditions is carried out. The primary frequency and difference frequency directivities measured at $z = 4$ m (Figure 7) away from the sound source are measured and compared with the numerical calculation. The results show that there was no significant difference between the sound pressure distributions through thin aluminum plate within a 10 degree. And, the beam width on the difference frequency component in Figure 7(c) is wider than the theoretical prediction because the acoustic transmission coefficient of thin aluminum plates varies with frequency.

Figure 8 shows axial sound pressure distribution of parametric sound field through the thin aluminum plate. The difference frequency sound pressure measured at the plate position reduced much less than the primary frequency sound pressure because the actual transmission coefficient of the aluminum plate changes with the frequency. However, the difference frequency sound pressure begun to decrease, and the attenuation speed decreases as the distance increases.

5. Conclusion

In this paper, the existing normal incidence KZK model is generalized to the 3D inclined incident model. The sound field with the transmittance inclined plane boundary condition is numerically simulated by solving the transformed beam KZK equation with FDTD method, and the sound pressure distribution of the parametric beam at the center of the sound is given out. The pool experiment verifies the correctness of theoretical analysis and numerical calculation. The proposed transform KZK model can also be used to calculate and analyze the parametric sound field propagation characteristics under inclined incident multilayer media.

Data Availability

The data used to support the findings of this study are available from the corresponding author upon request.

Conflicts of Interest

The authors declare no conflicts of interest.

Authors' Contributions

All the authors made significant contributions to this work. Haisen Li and Jingxin Ma initiated the research and designed the method. Jianjun Zhu and Baowei Chen performed experiments to verify the method. Jingxin Ma analyzed the data and wrote the paper. Jianjun Zhu and Haisen Li revised the manuscript.

Acknowledgments

This work was supported by NSFC-Zhejiang Joint Fund for the Integration of Industrialization and Informatization (no. U1809212), the National Natural Science Foundation of China (no. 41606115), and the National Key Research and Development Program of China (nos. 2017YFC0306000 and 2018YFF0212203) grant funded by the Chinese government.

References

[1] P. J. Westervelt, "Parametric acoustic array," *The Journal of the Acoustical Society of America*, vol. 35, no. 4, pp. 535–537, 1963.

[2] M. B. Bennett and D. T. Blackstock, "Parametric array in air," *The Journal of the Acoustical Society of America*, vol. 57, no. 3, pp. 562–568, 1975.

[3] R. H. Mellen, D. G. Browning, and W. L. Konrad, "Parametric sonar transmitting array measurements," *The Journal of the Acoustical Society of America*, vol. 49, no. 3B, pp. 932–935, 1971.

[4] R. L. Rolleigh, "Difference frequency pressure within the interaction region of a parametric array," *The Journal of the Acoustical Society of America*, vol. 58, no. 5, pp. 964–971, 1975.

[5] J. Dybedal, A. Lovik, and O. Malmo, "The parametric array source and application of signal processing," in *Proceedings of the IEEE 1987 Ultrasonics Symposium*, pp. 735–740, Denver CO, USA, October 1987.

[6] P. J. Westervelt, C. H. Allen, and R. S. Lansil, "Nonlinear acoustic properties of screens," *The Journal of the Acoustical Society of America*, vol. 32, no. 7, p. 934, 1960.

[7] K. G. Foote, R. Patel, and E. Tenningen, "Target-tracking in a parametric sonar beam, with applications to calibration," in *Proceedings of the OCEANS 2010 MTS/IEEE SEATTLE*, pp. 1–7, Seattle, WA, USA, September 2010.

[8] M. Saleh and M. Rabah, "Seabed sub-bottom sediment classification using parametric sub-bottom profiler," *NRIAG Journal of Astronomy and Geophysics*, vol. 5, no. 1, pp. 87–95, 2016.

[9] T. Zhou, H. S. Li, J. J. Zhu, and Y. K. Wei, "A geoacoustic estimation scheme based on bottom backscatter signals from multiple angles," *Acta Physica Sinica*, vol. 63, no. 8, 2014.

[10] Z. Li, E. Fang, and S. Shi, "Study on the calculation method of the KZK equation for parametric array," in *Proceedings of the 12th International Conference on Signal Processing (ICSP)*, pp. 139–143, HangZhou, China, October 2014.

[11] N. G. Pace and R. V. Ceen, "Time domain study of the terminated transient parametric array," *The Journal of the Acoustical Society of America*, vol. 73, no. 6, pp. 1972–1978, 1983.

[12] Y. S. Lee and M. F. Hamilton, "Time-domain modeling of pulsed finite-amplitude sound beams," *The Journal of the Acoustical Society of America*, vol. 97, no. 2, pp. 906–917, 1995.

[13] X. Yang and R. O. Cleveland, "Time domain simulation of nonlinear acoustic beams generated by rectangular pistons with application to harmonic imaging," *The Journal of the Acoustical Society of America*, vol. 117, no. 1, pp. 113–123, 2005.

[14] G. C. Gaunaurd and H. C. Strifors, "Frequency- and time-domain analysis of the transient resonance scattering resulting from the interaction of a sound pulse with submerged elastic shells," *IEEE Transactions on Ultrasonics, Ferroelectrics and Frequency Control*, vol. 40, no. 4, pp. 313–324, 1993.

[15] H. Nomura, C. M. Hedberg, and T. Kamakura, "Numerical simulation of parametric sound generation and its application to length-limited sound beam," *Applied Acoustics*, vol. 73, no. 12, pp. 1231–1238, 2012.

[16] K. Fujisawa and A. Asada, "Nonlinear parametric sound enhancement through different fluid layer and its application to noninvasive measurement," *Measurement*, vol. 94, pp. 726–733, 2016.

[17] X. Liu, J. Li, C. Yin, X. Gong, D. Zhang, and H. Xue, "The transmission of finite amplitude sound beam in multi-layered biological media," *Physics Letters A*, vol. 362, no. 1, pp. 50–56, 2007.

[18] S. L. Liu, Y. Y. Yang, C. H. Li, X. S. Guo, J. Tu, and D. Zhang, "Prediction of HIFU propagation in a dispersive medium via khokhlov-Zabolotskaya-kuznetsov model combined with a fractional order derivative," *Applied Sciences-Basel*, vol. 8, no. 4, 2018.

[19] J. Zhu, H. Li, B. Chen, and J. Ma, "Steered nonlinear field computation and measurement," in *Proceedings of the OCEANS 2015-MTS/IEEE Washington*, pp. 1–5, Washington, DC, USA, June 2015.

[20] F. Vander Meulen and L. Haumesser, "Layer contributions to the nonlinear acoustic radiation from stratified media," *Ultrasonics*, vol. 72, pp. 34–41, 2016.

[21] K. Fujisawa and A. Asada, "Numerical and experimental studies on nonlinear parametric sound enhancement through different fluid layers," *Wave Motion*, vol. 75, pp. 13–24, 2017.